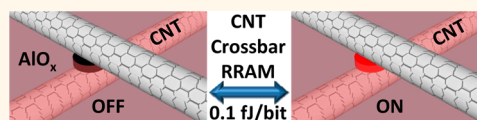


# Resistive Random Access Memory Enabled by Carbon Nanotube Crossbar Electrodes

Cheng-Lin Tsai,<sup>†,\*</sup> Feng Xiong,<sup>§,||,⊥</sup> Eric Pop,<sup>§,||,⊥</sup> and Moonsub Shim<sup>†,\*</sup>

<sup>†</sup>Department of Materials Science and Engineering, <sup>‡</sup>Frederic Seitz Materials Research Laboratory, <sup>§</sup>Department of Electrical and Computer Engineering, <sup>||</sup>Micro and Nanotechnology Laboratory, and <sup>⊥</sup>Beckman Institute, University of Illinois, Urbana, Illinois 61801, United States

**ABSTRACT** We use single-walled carbon nanotube (CNT) crossbar electrodes to probe sub-5 nm memory domains of thin  $\text{AlO}_x$  films. Both metallic and semiconducting CNTs effectively switch  $\text{AlO}_x$  bits between memory states with high and low resistance. The low-resistance state scales linearly with CNT series resistance down to  $\sim 10 \text{ M}\Omega$ , at which point the ON-state resistance of the  $\text{AlO}_x$  filament becomes the limiting factor. Dependence of switching behavior on the number of cross-points suggests a single channel to dominate the overall characteristics in multi-crossbar devices. We demonstrate ON/OFF ratios up to  $5 \times 10^5$  and programming currents of 1 to 100 nA with few-volt set/reset voltages. Remarkably low reset currents enable a switching power of 10–100 nW and estimated switching energy as low as 0.1–10 fJ per bit. These results are essential for understanding the ultimate scaling limits of resistive random access memory at single-nanometer bit dimensions.



**KEYWORDS:** carbon nanotubes · resistive memory · RRAM scaling · crossbar · atomic layer deposition (ALD) · aluminum oxide

Increasing data storage demands in computing, imaging, and mobile electronics are necessitating the development of memories that continue to push the limits in storage density, operation speed, and low power consumption.<sup>1</sup> Among several non-volatile memory candidates, resistive random access memory (RRAM) has attracted much attention because of its potential for high performance, scalability, and facile integration into current silicon-based CMOS technology.<sup>2,3</sup> In addition, resistive switching behavior observed in a wide variety of materials including metal oxides,<sup>2,4–9</sup> organics,<sup>10,11</sup> and nanocomposites<sup>12</sup> along with flexible device designs (*e.g.*, lateral<sup>11,13</sup> vs vertical<sup>2,4</sup> bits) and electrode materials<sup>14–17</sup> makes RRAMs promising for device integration and performance optimization. However, most current RRAMs utilize conventional lithographic processes for fabricating metal electrodes, which define the active switching area and therefore limit the memory density.<sup>2</sup> Due to their exceptional electrical, thermal, and mechanical properties, carbon nanotubes (CNTs), in particular single-walled CNTs, are attractive as electrode materials.<sup>10,11,18–23</sup> Their nanometer dimensions (*e.g.*, diameter 1–2 nm) are also useful in providing insights into fundamental RRAM scaling limits, as

metal electrodes are very difficult to pattern at sub-10 nm dimensions.<sup>11</sup> In addition, recent progress in the growth of nearly perfectly aligned CNTs on quartz substrates<sup>24</sup> along with transfer and integration techniques onto arbitrary substrates<sup>25</sup> may provide a feasible route toward ultrahigh-density high-performance RRAMs using CNT electrodes.

Here, we fabricate and examine CNT/ $\text{AlO}_x$ /CNT RRAMs with single to a few CNT–CNT cross-points. We observe that the low-resistance state (LRS) of the bits scales linearly with the higher resistance CNT electrode down to about 10 M $\Omega$ ; the high-resistance state (HRS) is independent of the resistance of the CNT electrodes and is dictated by the resistance of the  $\text{AlO}_x$  in its OFF state. The lower limit for the LRS in these devices is likely due to the resistance of  $\text{AlO}_x$  in its ON state (*i.e.*, the resistance of the individual nanoscale conducting filament in the  $\text{AlO}_x$ ). These CNT/ $\text{AlO}_x$ /CNT vertical RRAM devices exhibit reset currents as low as 1 nA and ON/OFF ratios up to  $5 \times 10^5$ . Dependence on the number of cross-points suggests that a single cross-point dictates the switching behavior even in devices with tens of cross-points. Both metallic and semiconducting CNTs (the latter often exhibiting higher resistance) are found

\* Address correspondence to mshim@illinois.edu.

Received for review March 10, 2013 and accepted May 25, 2013.

Published online May 25, 2013  
10.1021/nn401212p

© 2013 American Chemical Society

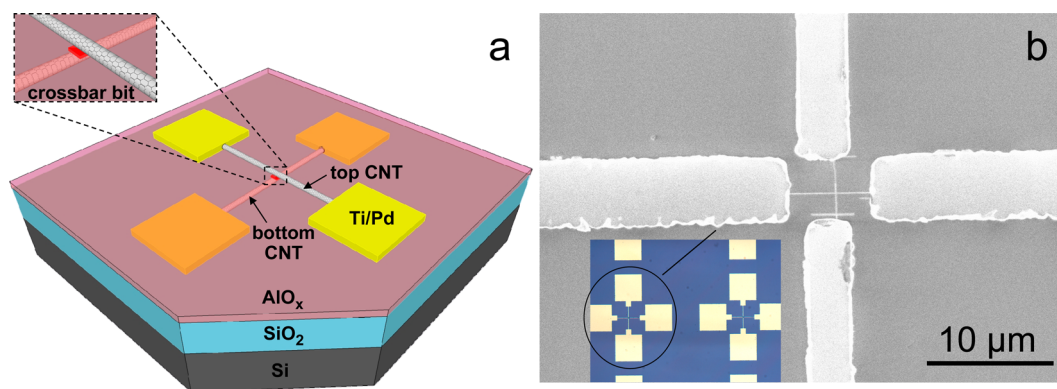


**Figure 1.** (a) Schematic of carbon nanotube (CNT) crossbar electrodes with  $\text{AlO}_x$  resistive random access memory (RRAM) bit at their intersection. (b) Scanning electron micrograph (SEM) of the RRAM bit structure, including metal contacts to CNTs. Inset shows optical image of adjacent fabricated crossbar devices. The distance between each Ti/Pd contact pair is  $\sim 7 \mu\text{m}$ , and the  $\text{AlO}_x$  film thickness is  $\sim 5.5 \text{ nm}$ .

to effectively switch  $\text{AlO}_x$ . Optimizing CNT resistance, especially with semiconducting CNTs, can simultaneously provide high ON/OFF ratios and low programming currents along with a built-in series resistance to reduce the possibility of permanent  $\text{AlO}_x$  breakdown and premature device failure. Semiconducting CNTs could also facilitate direct integration of selector devices that prevent crosstalk between memory cells<sup>26,27</sup> in future designs of these and related crossbar RRAMs. Moreover, the use of CNTs as nanoscale electrodes provides insights into the fundamental scaling limits of RRAM technology.

## RESULTS AND DISCUSSION

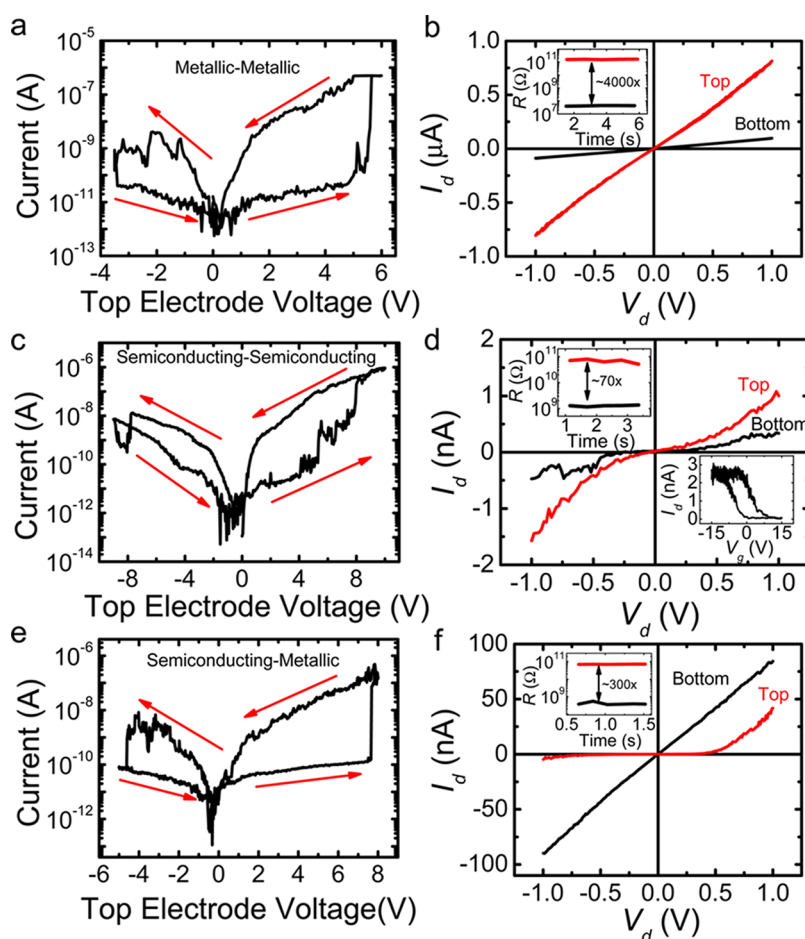
An example of devices prepared in this work is shown in Figure 1. These RRAMs consist of crossbar electrodes of horizontally aligned CNTs sandwiching thin ( $\sim 5.5 \text{ nm}$ )  $\text{AlO}_x$  films. The top and bottom layers of CNT electrodes are contacted by separate Ti/Pd pads (see Methods section for full fabrication details). We use  $\text{AlO}_x$  as the resistive switching medium in this work because it is commonly available and compatible with CNTs and we have found that it provides better switching characteristics than other comparable films we have experimented with (*e.g.*,  $\text{TiO}_x$ ). Nevertheless, our choice represents a first step, but does not rule out the future use of other materials as the switching medium between CNT crossbars, to be pursued in other studies.

Figure 2a shows the bipolar switching behavior of a CNT/ $\text{AlO}_x$ /CNT device consisting of metallic CNTs for both top and bottom electrodes (one on bottom and two on top, leading to a total of two CNT–CNT crosspoints, as verified by atomic force microscopy; not shown). A current compliance of  $1 \mu\text{A}$  was imposed for the forming step and the set operations as usually recommended for operations of most RRAMs.<sup>2</sup> No compliance was imposed for the reset operation. Despite an apparent symmetric CNT/ $\text{AlO}_x$ /CNT geometry, bipolar behavior can be expected here since the top and the bottom CNTs may have different

resistances. This device exhibits reasonable set/reset voltages ( $+5.5/-3.5 \text{ V}$ ) after the initial forming step at  $\sim 8 \text{ V}$ . This slightly higher forming voltage is consistent with most metal-oxide RRAMs<sup>2,4</sup> and is necessary to initiate subsequent resistive switching behavior. The set/reset voltages of crossbar RRAMs fabricated here remain stable within *ca.*  $\pm 0.5 \text{ V}$ . Within our measurement time of  $12\,500 \text{ s}$ , good retention is demonstrated for this device in the Supporting Information (Figure S1a). However, some degradation in the ON/OFF ratio is observed over 50 cycles (Figure S1b), suggesting approaches such as encapsulation may be necessary to improve endurance.

Our four-contact pad configuration allows us to measure current–voltage ( $I$ – $V$ ) characteristics of top and bottom CNTs separately, as shown in Figure 2b. Both CNT electrodes show ohmic or near-ohmic behavior in this particular case (*i.e.*, metallic or sufficiently doped semiconducting CNTs). The HRS in Figure 2a can be described reasonably well by  $\log(I) \approx V^{1/2}$ , which is consistent with but does not necessarily confirm a Schottky emission-type conduction mechanism.<sup>29,30</sup> We note that the HRS does not exhibit a pronounced asymmetry (like a typical Schottky diode) either due to near symmetric CNT/ $\text{AlO}_x$ /CNT device structure or, more likely, due to the high resistance of the  $\text{AlO}_x$  OFF state dominating the overall resistance. The LRS value ( $\sim 40 \text{ M}\Omega$ ) is close to that of the more resistive CNT electrode, the bottom one in this case. This device shows a remarkably low reset current of  $\sim 10 \text{ nA}$  with a large ON/OFF ratio of  $\sim 4000$ .

Using similar CNT–CNT as well as metal (Al) line–CNT crossbar electrodes, Wu *et al.*<sup>22</sup> recently demonstrated  $\text{AlO}_x$  RRAMs with low programming currents and good endurance ( $>10^4$  cycles). Interestingly, they found that an Al/ $\text{AlO}_x$ /CNT configuration with a larger active area of  $\sim 40 \text{ nm} \times 1 \mu\text{m}$  exhibited a lower programming current ( $\sim 1 \mu\text{A}$ ) and voltage than the CNT/ $\text{AlO}_x$ /CNT configuration, for which the authors estimated an active area of only  $\sim 6 \times 6 \text{ nm}$  (by assuming semiconducting CNTs do not contribute as active electrodes). While vertical RRAMs



**Figure 2.** Switching behavior of  $\text{AlO}_x$  RRAMs with (a) metallic–metallic, (c) semiconducting–semiconducting, and (e) semiconducting–metallic top–bottom CNT crossbar electrodes. (b, d, f) Corresponding  $I$ – $V$  characteristics of top (red) and bottom (black) CNTs. The sharp current rise in the top electrode voltage  $>0$  V sweep represents the set process, and the sharp current drop in the top electrode voltage  $<0$  V sweep represents the reset process. “Jumps” in the current prior to switching (e.g., near  $-2.5$  V for the LRS in part (a)) are noise, which may be due to dynamic competition between set and reset process.<sup>28</sup> The bottom electrode is typically more resistive, most likely due to changes (decrease) in p-doping after  $\text{AlO}_x$  deposition (Figure 3). Top-left insets in (b), (d), and (f) show the ON/OFF ratio of the RRAM device measured with a top electrode voltage of 1.5 V. The bottom-right inset in part (d) shows the transfer characteristics of the bottom semiconducting CNT (bottom right) at  $V_d = 50$  mV.

can have a much reduced bit area and therefore improved characteristics compared to lateral CNT RRAMs (e.g., those fabricated on  $\text{SiO}_2$  by electrical breakdown<sup>13</sup>), the crossbar RRAMs of Wu *et al.*<sup>22</sup> contained tens of CNTs per contact pad, which led to hundreds of CNT–CNT cross-points, complicating the switching process. This challenge, along with different  $\text{AlO}_x$  thickness, may explain the higher programming currents in their devices compared to ours. Wu *et al.*<sup>22</sup> also assumed that semiconducting CNTs did not contribute to the memory operation. However, semiconducting CNTs are typically the predominant electronic type in these aligned single-walled CNT arrays<sup>24</sup> as well as in most growth methods currently used. Hence, understanding how the presence of semiconducting CNTs affects the performance of RRAMs, or any device that utilizes CNTs as electrodes, is of critical importance.

Figure 2c shows the switching behavior of an RRAM device with semiconducting CNT electrodes and three CNT cross-points. The semiconducting nature of the bottom electrode is confirmed by the transfer characteristics

shown in the inset of Figure 2d. The top electrode consists of three CNTs that we expect to also be all semiconducting (as suggested by  $I$ – $V$  characteristics in Figure 2d, showing nonlinear behavior with fairly high resistance). Despite the relatively high resistance,  $\text{AlO}_x$  can be successfully switched with these semiconducting CNT electrodes with similar parameters, albeit slightly higher voltages, as the device with metallic CNT electrodes shown in Figure 2a. We observe set/reset voltages of  $+8/-8$  V and a reset current of only  $\sim 13$  nA. However, unlike the metallic CNT-based RRAM of Figure 2a and b, this device exhibits a smaller ON/OFF ratio of  $\sim 70$ . This difference arises from the fact that the HRS, which is dictated by the OFF-state  $\text{AlO}_x$  resistance (and independent of CNT electrode resistance), is similar for both devices, whereas the LRS, in most cases, is largely determined by the CNT electrode with higher resistance, as discussed below.

For completeness, the switching behavior and  $I$ – $V$  characteristics of a device with semiconducting–metallic

CNT top–bottom electrodes are shown in Figure 2e and f. This device with a semiconducting–metallic CNT electrode pair exhibits characteristics that appear to be more similar to the semiconducting–semiconducting case rather than the metallic–metallic case described above. That is, the higher resistance semiconducting top CNT electrode leads to higher set/reset voltages with a lower ON/OFF ratio. These similarities and differences between metallic and semiconducting CNT crossbar RRAMs distinguish our devices from recently reported two-terminal semiconducting CNT memories, which rely on charge migration between CNTs and substrates.<sup>23</sup> For example, devices relying on substrate charging effects in ref 23 undergo significant recovery within a few hours of switching (*cf.* Figure S1a, where we observe no significant recovery over several hours) and require set/reset voltages that are opposite in polarity compared with devices developed here when using p-type semiconducting CNTs. More strikingly, devices in ref 23 can be achieved only using semiconducting CNTs, whereas our devices can use both metallic and semiconducting CNTs with a larger ON/OFF ratio for metallic CNTs.

While it is promising that both metallic and semiconducting CNTs can effectively switch  $\text{AlO}_x$ , large device-to-device performance variations require a better understanding of how the CNT electronic type influences device operation. To this end, we have first examined how ALD deposition of  $\text{AlO}_x$  affects electrical characteristics of CNTs. When the top and the bottom electrodes consist of the same number of CNTs, we observe that the electrode underneath the  $\text{AlO}_x$  film usually exhibits higher resistance than the top electrode. One cause of this observation is the possible damage to CNTs from the  $\text{AlO}_x$  deposition process. However, our Raman measurements do not show any significant increase in the D-band of the bottom CNTs, indicating that little or no physical damage occurs (Supplementary Figure S2, inset). What is noticeable is the downshift of the G-band position after  $\text{AlO}_x$  deposition, as shown in Figure 3. This downshift along with the threshold shift to a more negative voltage seen in the inset of Figure 3 indicates that the doping level of the bottom CNT is changing. In other words, CNTs usually start as p-type and become less so upon  $\text{AlO}_x$  deposition. Similar doping changes have also been observed with ALD  $\text{AlO}_x$  deposition on CNT networks.<sup>31</sup> In metallic CNTs, the downshift in the G-band position is accompanied by a significant line broadening (Figure S2), which is the expected result of Fermi level position shifting toward the charge neutrality or the Dirac point, where carrier excitations become strongly coupled to the G-band phonons.<sup>32–37</sup> However, the conductivity of metallic CNTs is not affected much by this Fermi level position change, whereas semiconducting CNTs are turned off (or become less conducting) at zero back-gate voltage due to this “undoping” effect. These results suggest that one way to improve performances of devices consisting of

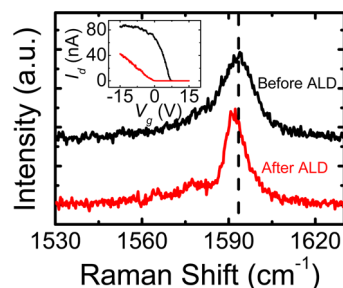


**Figure 3.** G-Band Raman spectra and transfer characteristics (inset,  $V_d = 50$  mV) of a semiconducting CNT before (black) and after (red) atomic layer deposition (ALD) of  $\sim 5.5$  nm  $\text{AlO}_x$ . The G-band shifts left after  $\text{AlO}_x$  deposition, signifying a change in doping that “turns off” the CNT at zero back-gate voltage  $V_g$  (see inset). The Raman spectra are vertically offset for clarity. The dashed line is included as a guide line.

semiconducting CNTs is to ensure sufficient doping, *e.g.*, by choice of the substrate or the switching material. However, as discussed later, maintaining sufficient electrical resistance in the CNT electrodes could also be beneficial in preventing premature breakdown of the  $\text{AlO}_x$  bits.

In order to gain insights into the impact of a combination of semiconducting and metallic CNTs on RRAM device operation and scaling behavior, we consider here the variations in the HRS/LRS resistances and set/reset voltages. The HRS is independent of CNT electronic type, and the number of cross-points within a device and the resistance values are  $>10$  G $\Omega$  (Figures S3 and 4a), similar to that of a control device without any CNTs (*i.e.*, metal pads and  $\text{AlO}_x$ , as shown in Figure 1, but without the presence of the CNTs). On the other hand, the LRS and the set/reset voltages appear to have some dependence on the CNT electronic type, with metallic–metallic CNT–CNT crossbars exhibiting the lowest resistances and voltages and semiconducting–semiconducting cases exhibiting the highest (Figure S3). Within the range of the number of CNT–CNT junctions examined (1 to 40), the LRS shows no obvious dependence on the number of CNT cross-points other than increasing scatter in the data as the number of cross-points approach 1 and the minimum resistance value of  $\sim 10$  M $\Omega$  being independent of the number of cross-points (Figure 4). Set and reset voltages also exhibit similar trend in the scatter and the minimum voltage value with number of CNT–CNT junctions. These results combined with CNT electrode resistance dependence discussed below suggest that a single cross-point, independent of the number of CNT–CNT junctions, determines the switching characteristics of these RRAMs. Hence, despite the variations in CNT electronic type and the number of cross-points, all devices fabricated here exhibited a very small programming current of  $\sim 1$  to 100 nA and switching power of 6 to 700 nW (Figure S4).

Similar to the trends with CNT electronic type and the number of cross-points, Figure 5a shows that the HRS is also independent of the resistances of CNT



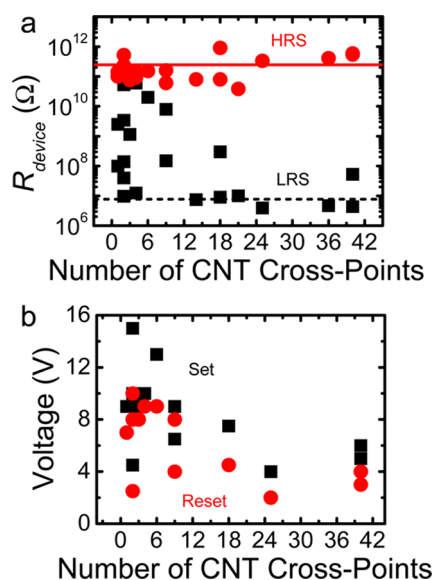


**Figure 4.** (a) Crossbar RRAM resistance of HRS (red circles) and LRS (black squares) and (b) set (black squares) and reset (red circles) voltages as a function of the number of CNT cross-points. Only devices that can undergo multiple switching cycles are plotted in part (b).

electrodes. However, the LRS exhibits stronger dependence on the resistance of the more resistive CNT electrode than the electronic type or the number of cross-points. Both set/reset voltages also show significant dependence on the CNT electrode resistance, scaling approximately linearly with CNT electrode resistance, as shown in Figure 5b. The slight dependence of LRS seen with electronic type (Figure S3) is due to the fact that semiconducting CNTs usually exhibit higher resistance because they are not fully “turned on”. The LRS shows linear dependence on the higher resistance CNT electrode down to approximately 10 M $\Omega$ . The solid black line in Figure 5a has a slope of 1 and a y-intercept of 0, indicating that the LRS of these RRAMs is dominated by the CNT electrode resistance. That is, the resistances of the conducting filament in the AIO<sub>x</sub> and the interface between CNT and AIO<sub>x</sub> are negligible in this regime. The LRS becomes constant ( $\sim$ 10 M $\Omega$ , as indicated by the dashed line), independent of CNT electrode resistance, when the CNT electrode resistance of the device is less than  $\sim$ 10 M $\Omega$ . This limit occurs because when CNTs are sufficiently conductive, the resistance of the AIO<sub>x</sub> in its ON state (plus possible interfacial resistance), *i.e.*, of a single conducting filament in AIO<sub>x</sub>, dictates the device characteristics.

The constant LRS of  $\sim$ 10 M $\Omega$  in the limit of sufficiently conductive CNT electrodes (Figure 5a) and the increasing scatter in the LRS with decreasing number of cross-points (Figure 4a) can be explained by considering the overall switching behavior being determined by only a single CNT–CNT junction even if there are multiple cross-points. As the number of CNTs increases, the resistance of the most conductive CNT

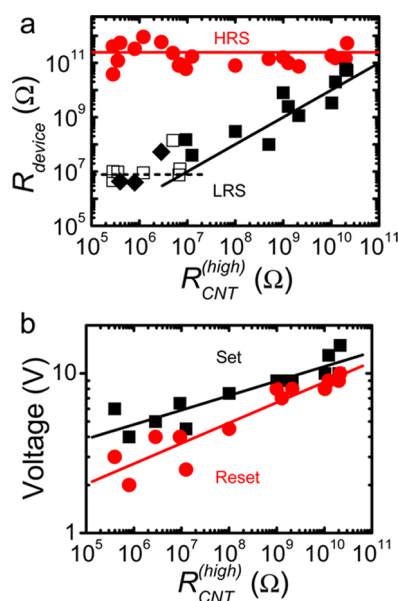


**Figure 5.** (a) Crossbar RRAM high-resistance state (HRS, red circles) and low-resistance state (LRS, black squares and diamonds) as a function of the resistance of the most resistive CNT electrode. The solid black line of slope 1 shows a one-to-one correspondence between the LRS and the CNT electrode resistance. The LRS becomes independent of CNT electrode resistance near 10 M $\Omega$ , as emphasized by the dashed line. The HRS is independent of CNT electrode resistance throughout the range examined (red line). Filled and open squares correspond to devices that used a compliance of 1  $\mu$ A for the initial forming step. Filled squares are the typical devices that can undergo multiple switching cycles, whereas open squares correspond to devices that cannot be switched back once turned on. Filled diamonds correspond to devices that were formed with a smaller 100 nA compliance. These devices span a similar CNT resistance range to the open-square devices, but exhibit multiple switching cycles. (b) Set (black squares) and reset (red circles) voltages of the RRAMs as a function of the more resistive CNT electrode resistance. The lines are linear fits.

will approach a similar low value, *i.e.*, < 10 M $\Omega$ . The least resistive path determined by the most conducting CNT, once switched ON, will make it much more difficult for other cross-points to be turned ON as well. A single active cross-point, despite the device having multiple CNT–CNT junctions, then leads to similar LRS determined by the resistance of a single conducting filament of the AIO<sub>x</sub> within that cross-point (*i.e.*,  $\sim$ 10 M $\Omega$ ). When there is only one or a very limited number of cross-points, the resistance of the most conductive CNT would vary widely from device to device, leading to a large variation in the LRS, which in many cases will be determined by the CNT resistance.

Devices that deviate from the linear dependence of LRS on CNT electrode resistance near 10 M $\Omega$  and below in Figure 5a provide further insights on device characteristics that may facilitate performance improvements. The filled and open squares correspond to devices that have undergone a forming step with a current compliance of 1  $\mu$ A. For these devices, when the CNT electrode resistance is greater than  $\sim$ 10 M $\Omega$ , the expected multiple switching behavior is observed

(filled squares). When the CNT electrodes are more conductive (*i.e.*, less than  $\sim 10$  M $\Omega$  in resistance), these devices cannot be switched multiple times and remain ON permanently (open squares). For some cases, a current of  $\sim 1$   $\mu$ A is sufficient to cause permanent breakdown of the small AlO<sub>x</sub> filament at the CNT cross-points during the forming step. Other devices have permanent breakdown occurring during the reset step. We do not impose a current compliance for the reset step, and current jumps larger than those of the forming step are observed when these devices break down. One way to avoid both types of breakdown is to impose a smaller current compliance during the forming step. The filled diamonds in Figure 5a correspond to devices with CNT electrode resistance less than  $\sim 10$  M $\Omega$  that have undergone the forming process with a compliance of 100 nA. These devices can be switched multiple times, similar to the devices with more resistive CNT electrodes.

These observations on the dependence of LRS on CNT electrode resistance and how current compliance affects permanent breakdown behavior suggest three important points. First, as discussed above, the  $\sim 10$  M $\Omega$  limit for the LRS being independent of the number of cross-points in a device may imply that even with multiple CNT cross-points there is likely to be only one active channel undergoing the switching event (the most conductive junction including CNT resistance). Second, CNT electrodes with a resistance higher than  $\sim 10$  M $\Omega$  behave as built-in series resistors that automatically set a current compliance preventing accidental permanent breakdown of these RRAMs. That is, choosing CNT electrodes with slightly higher resistance than that of the conducting filament within the AlO<sub>x</sub> layer provides a simple means to achieve devices without much sacrifice in power consumption and ON/OFF ratio. Third, our results suggest the resistance of a single conductive filament of 5.5 nm thick AlO<sub>x</sub> to be  $\sim 10$  M $\Omega$

at the intersection of two CNTs. This is an essential quantity for the future understanding of the scalability limits of such RRAM technology.

## CONCLUSIONS

In conclusion, we have demonstrated CNT/AlO<sub>x</sub>/CNT crossbar RRAMs with programming current as low as 1 nA and ON/OFF ratio up to  $5 \times 10^5$ . The HRS of these RRAMs is determined by the resistance of the thin AlO<sub>x</sub> in its OFF state, whereas the LRS is dictated by the resistance of the highest resistance CNT electrode until what appears to be the resistance of a single conducting filament is reached ( $\sim 10$  M $\Omega$  for 5.5 nm AlO<sub>x</sub>). This 10 M $\Omega$  limit for the LRS is independent of the number of cross-points and suggests that there is only a single active bit even if there are multiple CNT–CNT junctions. The varying resistances of CNT electrodes especially due to the presence of both metallic and semiconducting CNTs (and the varying degree of doping in semiconducting CNTs) cause variations in the ON/OFF ratio, which we observe to occur mostly in the small number of cross-points per device ( $< \sim 10$ ) regime. Nevertheless, all devices fabricated here exhibit very low reset currents (1–100 nA), with reset voltage ranging from 2 to 10 V. Using a switching time of  $\sim 10$  ns observed in AlO<sub>x</sub> RRAMs,<sup>9</sup> we estimate a switching energy of 60 to 7000 aJ per bit. While direct experimental verification is needed, these values suggest extremely low *intrinsic* switching energies for our CNT crossbar devices. Interestingly, devices with these promising characteristics include all-semiconducting CNT electrodes, which may also be a potentially useful option for introducing selector devices in these RRAMs. Finally, as we scale bit size down to  $\sim 5$  nm or smaller, AlO<sub>x</sub> appears to be more prone to premature breakdown. Using CNT electrodes with resistances slightly larger than the ON-state resistance of the AlO<sub>x</sub> bit ( $> 10$  M $\Omega$ ) leads to built-in series resistors that prevent such breakdowns without much sacrifice in performance.

## METHODS

Horizontally aligned CNTs were grown by chemical vapor deposition on ST-cut quartz (Hoffman Materials) using ferritin (Sigma-Aldrich) as catalyst and CH<sub>4</sub> as carbon source. Aligned CNTs grown on quartz were transferred onto SiO<sub>2</sub> (300 nm)/Si substrates in order to characterize the electrical properties of the arrays with the Si back-gate.<sup>38</sup> Lithographically patterned metal pads (2 nm of Ti and 50 nm of Pd) were deposited to define 7  $\mu$ m long CNT electrodes. CNTs outside this region were etched by O<sub>2</sub> plasma to isolate devices. Devices were subsequently annealed at 400 °C with Ar and H<sub>2</sub> flow to ensure good contact between the metal pads and the CNTs. For the resistive oxide layer, AlO<sub>x</sub> was chosen because of its well-established conformal film deposition by atomic layer deposition (ALD) as well as the low reset currents reported.<sup>2</sup> A  $\sim 5.5$  nm thick AlO<sub>x</sub> film was deposited by ALD using H<sub>2</sub>O and trimethylaluminum as precursors at 80 °C for 50 cycles ( $\sim 1.1$  Å/cycle).<sup>39</sup> A second layer of aligned CNTs was then transferred<sup>32</sup> perpendicular to the first CNT layer covered by AlO<sub>x</sub>. Lithographically defined electrodes were again deposited on the second CNT layer, and an isolation

pattern was defined to remove excess CNTs. No annealing was carried out for the second CNT layer to prevent device degradation of the first CNT layer and of the AlO<sub>x</sub> film. Using the Si back-gate, CNTs in the first layer were identified as metallic or semiconducting prior to AlO<sub>x</sub> deposition. Since we cannot independently gate the top CNT layer, we assume metallic (or sufficiently doped semiconducting) when linear current–voltage (*I*–*V*) characteristics were observed and semiconducting when nonlinear behavior was observed. All switching experiments were carried out at room temperature under vacuum ( $4 \times 10^{-5}$  Torr) with a Keithley 4200 semiconductor characterization system.

**Conflict of Interest:** The authors declare no competing financial interest.

**Acknowledgment.** This material is based upon work supported in part by the MSD Focus Center, under the Focus Center Research Program (FCRP), a Semiconductor Research Corporation entity, and in part by the NSF grants 09-05175 (M.S.) and 10-02026 (E.P.). Experiments were carried out in part in the Frederick Seitz Materials Research Laboratory Central Facilities, University of Illinois.

Supporting Information Available: Metallic CNT doping change before and after  $\text{AlO}_x$  deposition, device resistance and switching voltage with different CNT electronic types, device resistance and switching voltage with different number of CNT junctions, switching current and power statistics. This material is available free of charge via the Internet at <http://pubs.acs.org>.

## REFERENCES AND NOTES

- Meijer, G. I. Who Wins the Nonvolatile Memory Race? *Science* **2008**, *319*, 1625–1626.
- Wong, H.-S. P.; Lee, H.-Y.; Yu, S.; Chen, Y.-S.; Wu, Y.; Chen, P.-S.; Lee, B.; Chen, F. T.; Tsai, M.-J. Metal-Oxide RRAM. *Proc. IEEE* **2012**, *100*, 1951–1970.
- Zhirnov, V. V.; Meade, R.; Cavin, R. K.; Sandhu, G. Scaling Limits of Resistive Memories. *Nanotechnology* **2011**, *22*, 254027–254048.
- Waser, R.; Dittmann, R.; Staikov, G.; Szot, K. Redox-Based Resistive Switching Memories Nanoionic Mechanisms, Prospects, and Challenges. *Adv. Mater.* **2009**, *21*, 2632–2663.
- Jeong, H. Y.; Lee, J. Y.; Choi, S.-Y. Interface-Engineered Amorphous  $\text{TiO}_2$ -Based Resistive Memory Devices. *Adv. Funct. Mater.* **2010**, *20*, 3912–3917.
- Yu, S.; Wu, Y.; Wong, H.-S. P. Investigate the Switching Dynamics and Multilevel Capability of Bipolar Metal Oxide Resistive Switching Memory. *Appl. Phys. Lett.* **2011**, *98*, 103514.
- Li, M.; Zhuge, F.; Zhu, X.; Yin, K.; Wang, J.; Liu, Y.; He, C.; Chen, B.; Li, R.-W. Nonvolatile Resistive Switching in Metal/La-doped  $\text{BiFeO}_3/\text{Pt}$  Sandwiches. *Nanotechnology* **2010**, *21*, 425202–425407.
- Xu, N.; Liu, L.; Sun, X.; Liu, X.; Han, D.; Wang, Y.; Han, R.; Kang, J.; Yu, B. Characteristics and Mechanism of Conduction/Set Process in  $\text{TiN}/\text{ZnO}/\text{Pt}$  Resistance Switching Random-Access Memories. *Appl. Phys. Lett.* **2008**, *92*, 232112.
- Wu, Y.; Yu, S.; Lee, B.; Wong, H.-S. P. Low-Power  $\text{TiN}/\text{Al}_2\text{O}_3/\text{Pt}$  Resistive Switching Device with Sub-20  $\mu\text{A}$  Switching Current and Gradual Resistance Modulation. *J. Appl. Phys.* **2011**, *110*, 094104.
- Chai, Y.; Wu, Y.; Takei, K.; Chen, H.-Y.; Yu, S.; Chan, P. C. H.; Javey, A.; Wong, H.-S. P. Nanoscale Bipolar and Complimentary Resistive Switching Memory Based on Amorphous Carbon. *IEEE Trans. Electron Devices* **2011**, *58*, 3933–3939.
- Xiong, F.; Liao, A. D.; Estrada, D.; Pop, E. Low-Power Switching of Phase-Change Materials with Carbon Nanotube Electrodes. *Science* **2011**, *332*, 568–570.
- Hwang, S. K.; Lee, J. M.; Kim, S.; Park, J. S.; Park, H. I.; Ahn, C. W.; Lee, K. J.; Lee, T.; Kim, S. O. Flexible Multilevel Resistive Memory with Controlled Charge Trap B- and N-Doped Carbon Nanotubes. *Nano Lett.* **2012**, *12*, 2217–2221.
- Yao, J.; Zhong, L.; Zhang, Z.; He, T.; Jin, Z.; Wheeler, P. J.; Natelson, D.; Tour, J. M. Resistive Switching in Nanogap Systems on  $\text{SiO}_2$  Substrates. *Small* **2009**, *5*, 2910–2915.
- Lin, K.-L.; Hou, T.-H.; Shieh, J.; Lin, J.-H.; Chou, C.-T.; Lee, Y.-J. Electrode Dependence of Filament Formation in  $\text{HfO}_2$  Resistive-Switching Memory. *J. Appl. Phys.* **2011**, *109*, 084104.
- Chen, M.-C.; Chang, T.-C.; Tsai, C.-T.; Huang, S.-Y.; Chen, S.-C.; Hu, C.-W.; Sze, S. M.; Tsai, M.-J. Influence of Electrode Material on the Resistive Memory Switching Property of Indium Gallium Zinc Oxide Thin Films. *Appl. Phys. Lett.* **2010**, *96*, 262110.
- Lin, C.-Y.; Wu, C.-Y.; Wu, C.-Y.; Lee, T.-C.; Yang, F.-L.; Hu, C.; Tseng, T.-Y. Effect of Top Electrode Material on Resistive Switching Properties of  $\text{ZrO}_2$  Film Memory Devices. *IEEE Electron Device Lett.* **2007**, *28*, 366–368.
- Russo, U.; Cagli, C.; Spiga, S.; Cianci, E.; Ielmini, D. Impact of Electrode Materials on Resistive-Switching Memory Programming. *IEEE Electron Device Lett.* **2009**, *30*, 817–819.
- Xiong, F.; Liao, A. D.; Pop, E. Inducing Chalcogenide Phase Change with Ultra-Narrow Carbon Nanotube Heaters. *Appl. Phys. Lett.* **2009**, *95*, 243103.
- Aguirre, C. M.; Ternon, C.; Paillet, M.; Desjardins, P.; Martel, R. Carbon Nanotubes as Injection Electrodes for Organic Thin Film Transistors. *Nano Lett.* **2009**, *9*, 1457–1461.
- Agnus, G.; Zhao, W.; Derycke, V.; Filoramo, A.; Lhuillier, Y.; Lenfant, S.; Vuillaume, D.; Gamrat, C.; Bourgoin, J.-P. Two-Terminal Carbon Nanotube Programmable Devices for Adaptive Architectures. *Adv. Mater.* **2010**, *22*, 702–706.
- Feldman, A. K.; Steigerwald, M. L.; Guo, X.; Nuckolls, C. Molecular Electronic Devices Based on Single-Walled Carbon Nanotube Electrodes. *Acc. Chem. Res.* **2008**, *41*, 1731–1741.
- Wu, Y.; Chai, Y.; Chen, H.-Y.; Yu, S.; Wong, H.-S. P. Resistive Switching  $\text{AlO}_x$ -Based Memory with CNT Electrode for Ultra-Low Switching Current and High Density Memory Application. *Symp. VLSI Technol.* **2011**, 26–27.
- Yao, J.; Jin, Z.; Zhong, L.; Natelson, D.; Tour, J. M. Two-Terminal Nonvolatile Memories Based on Single-Walled Carbon Nanotubes. *ACS Nano* **2009**, *3*, 4122–4126.
- Kang, S. J.; Kocabas, C.; Ozel, T.; Shim, M.; Pimparkar, N.; Alam, A.; Rotkin, S. V.; Rogers, J. A. High-Performance Electronics Using Dense, Perfectly Aligned Arrays of Single-Walled Carbon Nanotubes. *Nat. Nanotechnol.* **2007**, *2*, 230–236.
- Kang, S. J.; Kocabas, C.; Kim, H.-S.; Cao, Q.; Meitl, M. A.; Khang, D.-Y.; Rogers, J. A. Printed Multilayer Superstructures of Aligned Single-Walled Carbon Nanotubes for Electronic Applications. *Nano Lett.* **2007**, *7*, 3343–3348.
- Shin, J.; Kim, I.; Biju, K. P.; Jo, M.; Park, J.; Lee, J.; Jung, S.; Lee, W.; Kim, S.; Park, S.; et al.  $\text{TiO}_2$ -Based Metal-Insulator-Metal Selection Device for Bipolar Resistive Random Access Memory Cross-Point Application. *J. Appl. Phys.* **2011**, *109*, 033712.
- Huang, Y.; Huang, R.; Pan, Y.; Zhang, L.; Cai, Y.; Yang, G.; Wang, Y. A New Dynamic Selector Based on the Bipolar RRAM for the Crossbar Array Application. *IEEE Trans. Electron Devices* **2012**, *59*, 2277–2280.
- Yao, J.; Zhong, L.; Natelson, D.; Tour, J. M. In Situ Imaging of the Conducting Filament in a Silicon Oxide Resistive Switching. *Sci. Rep.* **2012**, *2*, 242.
- Lin, C.-Y.; Wang, S.-Y.; Lee, D.-Y.; Tseng, T.-Y. Electrical Properties and Fatigue Behaviors of  $\text{ZrO}_2$  Resistive Switching Thin Films. *J. Electrochem. Soc.* **2008**, *155*, H615–H619.
- Wei, Z.; Kanzawa, Y.; Arita, K.; Katoh, Y.; Kawai, K.; Muraoka, S.; Mitani, S.; Fujii, S.; Katayama, K.; Iijima, M.; et al. Highly Reliable  $\text{TaO}_x$  ReRAM and Direct Evidence of Redox Reaction Mechanism. *Tech. Dig.-IEEE Int. Electron Devices Meeting* **2008**, 293–296.
- Zhang, J.; Wang, C.; Fu, Y.; Che, Y.; Zhou, C. Air-Stable Conversion of Separated Carbon Nanotube Thin-Film Transistors from P-type to N-type Using Atomic Layer Deposition of High-k Oxide and Its Application in CMOS Logic Circuits. *ACS Nano* **2011**, *5*, 3284–3292.
- Nguyen, K. T.; Gaur, A.; Shim, M. Fano Lineshape and Phonon Softening in Single Isolated Metallic Carbon Nanotubes. *Phys. Rev. Lett.* **2007**, *98*, 145504.
- Piscanec, S.; Lazzeri, M.; Mauri, F.; Ferrari, A. C.; Robertson, J. Kohn Anomalies and Electron-Phonon Interactions in Graphite. *Phys. Rev. Lett.* **2004**, *93*, 185503.
- Das, A.; Sood, A. K.; Govindaraj, A.; Saitta, A. M.; Lazzeri, M.; Mauri, F.; Rao, C. N. R. Doping in Carbon Nanotubes Probed by Raman and Transport Measurements. *Phys. Rev. Lett.* **2007**, *99*, 136803.
- Wu, Y.; Maultzsch, J.; Knoesel, E.; Chandra, B.; Huang, M.; Sfeir, M. Y.; Brus, L. E.; Hone, J.; Heinz, T. F. Variable Electron-Phonon Coupling in Isolated Metallic Carbon Nanotubes Observed by Raman Scattering. *Phys. Rev. Lett.* **2007**, *99*, 027402.
- Farhat, H.; Son, H.; Samsonidze, G. G.; Reich, S.; Dresselhaus, M. S.; Kong, J. Phonon Softening in Individual Metallic Carbon Nanotubes Due to the Kohn Anomaly. *Phys. Rev. Lett.* **2007**, *99*, 145506.
- Tsang, J. C.; Freitag, M.; Perebeinos, V.; Liu, J.; Avouris, Ph. Doping and Phonon Renormalization in Carbon Nanotubes. *Nat. Nanotechnol.* **2007**, *2*, 725.
- Tsai, C.-L.; Liao, A.; Pop, E.; Shim, M. Electrical Power Dissipation in Semiconducting Carbon Nanotubes on Single Crystal Quartz and Amorphous  $\text{SiO}_2$ . *Appl. Phys. Lett.* **2011**, *99*, 053120.
- George, S. M. Atomic Layer Deposition: An Overview. *Chem. Rev.* **2010**, *110*, 111–131.